Title

Humpback whale-generated ambient noise levels provide insight into singers' spatial densities

Journal

The Journal of the Acoustical Society of America, 140(3)

ISSN

0001-4966

Authors

Seger, Kerri D
Thode, Aaron M
Urban-R., Jorge
et al.

Publication Date

2016-09-01

DOI

10.1121/1.4962217

Peer reviewed

Humpback whale-generated ambient noise levels provide insight into singers' spatial densities

Kerri D. Seger[a] and Aaron M. Thode
Scripps Institution of Oceanography, University of California San Diego, 9500 Gilman Drive, Mail Code 0206, La Jolla, California 92093, USA

Jorge Urbán-R., Pamela Martínez-Loustalot, M. Esther Jiménez-López, and Diana López-Arzate
Laboratorio de Mamíferos Marinos, Universidad Autónoma de Baja California Sur, Carretera Sur km 5.5, Apartado Postal 19-B, 23080, La Paz, Mexico

(Received 28 September 2015; revised 26 July 2016; accepted 13 August 2016; published online 8 September 2016)

Baleen whale vocal activity can be the dominant underwater ambient noise source for certain locations and seasons. Previous wind-driven ambient-noise formulations have been adjusted to model ambient noise levels generated by random distributions of singing humpback whales in ocean waveguides and have been combined to a single model. This theoretical model predicts that changes in ambient noise levels with respect to fractional changes in singer population (defined as the noise "sensitivity") are relatively unaffected by the source level distributions and song spectra of individual humpback whales (*Megaptera novaeangliae*). However, the noise "sensitivity" does depend on frequency and on how the singers' spatial density changes with population size. The theoretical model was tested by comparing visual line transect surveys with bottom-mounted passive acoustic data collected during the 2013 and 2014 humpback whale breeding seasons off Los Cabos, Mexico. A generalized linear model (GLM) estimated the noise "sensitivity" across multiple frequency bands. Comparing the GLM estimates with the theoretical predictions suggests that humpback whales tend to maintain relatively constant spacing between one another while singing, but that individual singers either slightly increase their source levels or song duration, or cluster more tightly as the singing population increases.
[http://dx.doi.org/10.1121/1.4962217]

[MS] Pages: 1581–1597

I. INTRODUCTION

To estimate the relative abundance and/or density of cetaceans, passive acoustic surveys complement visual surveys because they can be performed overnight or in inclement weather (Clark and Fristrup, 1997; Raftery and Zeh, 1998; Mellinger and Barlow, 2003; and Barlow and Taylor, 2005). However, acoustics alone (after verification using visuals) could be used to estimate the overall abundance and/or growth rates of marine animal populations within protected regions (Raftery and Zeh, 1998).

The use of passive acoustic monitoring to estimate population densities of animals began by using cue rates in the terrestrial realm with mammals, amphibians, songbirds, bats, and insects (Dawson and Efford, 2009; Buckland, 2006; and Blumstein *et al.*, 2011). Such techniques have also been applied to the marine realm for fish (Lucskovich *et al.*, 2008) and cetaceans, such as Blainville's beaked whale (Marques *et al.*, 2009), the right whale (Marques *et al.*, 2011), the fin whale (McDonald and Fox, 1999), and the minke whale (Martin *et al.*, 2013). Marques *et al.* (2013) summarize recent literature on passive acoustic density estimation for cetaceans.

All the research cited above used individual call detections (cue rates) as a basis for marine mammal population estimates. However, during breeding seasons at certain locations, several baleen whale species—including the fin whale, blue whales (McCauley *et al.*, 2001), and the humpback whale (Au *et al.*, 2000)—vocalize so often that individual cue rates cannot be measured; instead, individual sounds blend together to create a diffuse and continuous din across species-specific frequency bands in the acoustic environment. In the case of humpback whales, proliferous singing activity from multiple animals overlaps to create this din and makes it impossible to tease apart separate song units (Fig. 1). Therefore, for the remainder this paper, the din created by humpback whale song will be referred to as "noise," even though it contains potential information about the population size.

Humpback whales use song and social calls on both feeding and breeding grounds, as well as along migration routes, to facilitate their behaviors (Sharpe, 2001; Dunlop *et al.*, 2008; Zoidis *et al.*, 2008; Stimpert *et al.*, 2011). Song is a male communication strategy that does occur on migration routes (Clapham and Mattila, 1990; Norris *et al.*, 1999; Charif *et al.*, 2001) and feeding grounds (Mattila *et al.*, 1987; Clark and Clapham, 2004; Stimpert *et al.*, 2012; Vu *et al.*, 2012), but is especially prevalent on breeding grounds. It was originally thought to serve as a means of attracting

[a]Electronic mail: kseger@ccom.unh.edu

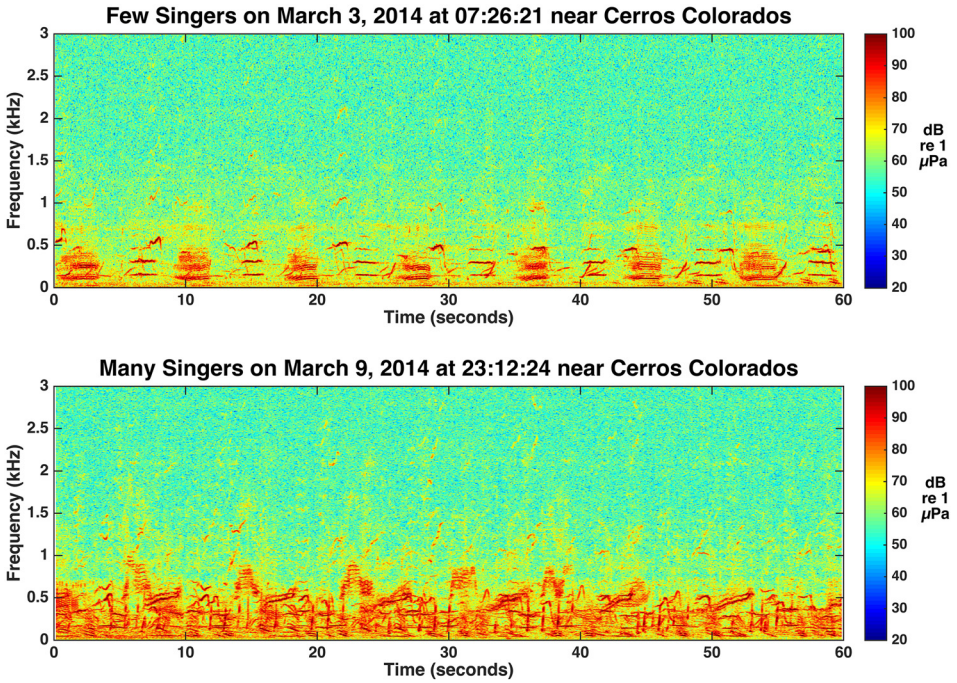

FIG. 1. (Color online) Ambient "noise" generated from humpback whale song varies throughout the day. Two 60-s spectrograms illustrate times of relatively low (top) and high (bottom) singing activity at Cerros Colorados in 2014 as recorded on an autonomous bottom-mounted hydrophone.

females (Payne and McVay, 1971; Winn and Winn, 1978; Tyack, 1981). Other theories reviewed by Darling and Bérubé (2001) include how song may serve as a mechanism for males to space themselves evenly from other singers (Tyack, 1981; Frankel *et al.*, 1995; Au *et al.*, 2000). If song contains information about spacing, then measuring its received intensity with knowledge of local sound transmission would contain information about the number of singers producing a certain singing level.

Au *et al.* (2000) was one of the first to propose that the diffuse ambient "humpback-generated noise" levels from many males singing together might be used to estimate their abundance. As part of the "DECAF" project sponsored by the Oil and Gas Producers' Association, Mellinger *et al.* (2009) developed a numerical model for estimating ambient noise levels generated by random distributions of fin whales.

In this paper we adapt existing analytic wind-driven ambient noise models to estimate the diffuse ambient noise levels that would be generated from random distributions of singing animals. Section II derives this theory, and defines a quantity dubbed the "sensitivity" of ambient noise measurements, in terms of how noise levels change with changes in relative population size. While this sensitivity is shown to be relatively independent of an individual humpback whale's source level or duty cycle, it does depend on acoustic frequency and on how the animals adjust their spatial density as their population increases. Section III describes the study area, equipment, procedures, and analyses used to test the analytic model, using combined acoustic and visual survey data collected in 2013 and 2014 from humpback whale breeding grounds off Los Cabos, México. Section IV compares the analytic model predictions of noise sensitivity with empirical estimates of sensitivity using a generalized linear model (GLM). Finally, we discuss how the results provide a connection between humpback whale behavioral adjustments with an increasing number of singers, and speculate about other species and environments where these methods might be useful.

II. THEORY AND SIMULATIONS

This section presents a theoretical model for the ambient noise field generated by a random distribution of singing whales (or any distribution of continuously vocalizing animals). It is a reinterpretation of previously derived analytic models of ambient noise levels generated by randomly distributed wind-driven breaking waves near the ocean surface. Given an acoustic propagation environment, and assuming various parameters about humpback whale singing behavior, the model predicts (1) ambient noise levels as a function of frequency and singer population size and (2) the "sensitivity" of ambient noise levels to changes in the singers' relative population size. As will be shown below, this sensitivity is relatively independent from the source levels and fraction of singing time (which will be referred to as duty cycles) assumed for a "typical" singing whale, but it depends strongly on how the spatial density of singers (or how they "pack" themselves) may change with fluctuations in population size.

A. Key features of the "KIP" model

Analytic models exist for ambient noise intensity in an ocean waveguide, given a distribution of random, uncorrelated noise sources throughout a finite ocean area (Kuperman and Ingenito, 1980; Perkins *et al.*, 1993; Jensen *et al.*, 1994). In the original Kuperman-Ingenito-Perkins (KIP) model (Appendix A), the acoustic sources were assumed to be wind-driven and just beneath the ocean surface. In this paper, however, we interpret the uncorrelated noise sources to be generated by a set of randomly distributed singing whales over a certain bandwidth. (Therefore, a fundamental assumption of the model is that the songs of all

animals are temporally uncorrelated over the time width of the window used to compute a power spectral density estimate.) The KIP model is general enough that the singers can be at any depth. However, to simplify the following discussion, it will be assumed that all singers are (1) singing at the same depth, (2) using a song that has equal and constant proportions of vocalizing and non-vocalizing times (i.e., the same "duty cycle"), (3) emitting the same and constant source levels, and (4) maintaining a constant spatial density within the effective radius. Appendix B shows that relaxing these assumptions (including introducing a linear gradient in spatial density) does not alter the fundamental points that are about to be discussed.

In essence, the KIP model has the following form:

$$I = \frac{Sf}{A(N)/N} P(z_w, z_r, R), \tag{1}$$

where I is the ambient noise intensity in terms of *linear* units of power spectral density (μPa^2/Hz, not dB). S is the source spectral density (in μPa^2/Hz @ 1 m) of a typical singing whale and is weighted by f: the fraction of singing time, or "duty cycle" (i.e., to account for times when a singer is not producing sound, such as the intervals between units and song cycles). N is the number of animals present in a region A that surrounds the recording hydrophone. [Equation (1) explicitly shows how this region A can depend on N.] The term $S/[A(N)/N]$ thus represents the average source intensity spectral density per unit area within the region A. Finally, the term $P(z_w,z_r,R)$ represents an acoustic propagation term that can be interpreted as a spatial average of the propagation losses between all possible singer positions at depth z_w within distance R of a receiver at depth z_r. R is the radius of the circular region A, centered over the bottom-mounted recorder. Appendix A also discusses situations where the receiver is in an arbitrary non-centered location with respect to the circular area.

P strongly depends on the acoustic propagation environment, including the water depth, ocean bottom composition, sound speed profile, and receiver depth. As a result, the marine mammal-generated ambient noise intensity produced by Eq. (1) is highly dependent on the ocean environment in which the animals are singing. For the purposes of this paper, a flat bathymetry for region A is assumed, but Perkins *et al.* (1993) discuss how the KIP model can be adapted to range-dependent bathymetries. Any water depth can be modeled, provided that the environment can be described in terms of a set of propagating normal modes. Appendix A presents the complete KIP model and discusses the collection of terms that comprise P in greater detail.

Equation (1) shows that ambient noise levels are directly proportional to the source intensity of a typical whale. If all whales in a region double their singing intensity, then ambient noise levels will double as well. Equation (1) also shows a direct proportionality between the ambient noise intensity and the spatial density of singers. For example, if the mean distance between singers halves, then both the spatial density and ambient noise spectral density will quadruple.

As Equation (A4) in Appendix A reveals, the P term in Eq. (1) asymptotically approaches some fixed value as R gets large (the area covered by singers increases to infinity), as long as the water has some sound absorbing properties. The reason P never becomes infinite is that noise contributions from singers at the edge of the circle contribute less and less to the sound field as the radius of the circle increases, despite the fact that the number of noise sources increases linearly with range. This means that ambient noise levels depend not only on the spatial density of singers, but also the physical size of region A. In terms of dB units ($10 * \log_{10}[]$), Eq. (1) can be expressed as

$$I_{dB} = S_{dB} + 10\log_{10} f + 10\log_{10} N - 10\log_{10} A + 10\log_{10} P, \tag{2}$$

where I_{dB} is the noise power spectral density level (dB re 1 μPa^2/Hz) and S_{dB} is the source level power spectral density (dB re 1 μPa^2/Hz @ 1 m) of a typical individual.

In principle, Eq. (2) could be used to estimate population density (N/A) from ambient noise level measurements, provided a random distribution is assumed, and one has sufficient knowledge about (1) the acoustic behavior of singers, including S, f, and z_w; (2) the propagation environment in terms of water depth, sound speed profile, and bottom composition; and (3) the actual geographic region of A (with effective radius R) that is occupied by singing animals.

Unfortunately, both S and f have large variations and uncertainties associated with them, which means that a large range of possible ambient noise levels exists for a given population density. Therefore, Sec. II B explores a more robust means of testing the KIP model that does not require assumptions about S and f.

B. The sensitivity of the ambient noise field to changes in singer population size

Equation (2) permits an estimate of the "sensitivity" of the ambient noise field to changes in population size. After converting to natural logs and cancelling factors of $\log_{10}e$, one takes the derivative of Eq. (2) with respect to the base-10 logarithm of population size N:

$$\delta \equiv \frac{\partial(I_{dB})}{\partial(10\log_{10} N)} = Q_{indiv} + 1 - \left(\frac{N}{A}\right)\frac{\partial A}{\partial N} + \left(\frac{N}{P}\right)\frac{\partial P}{\partial N}. \tag{3}$$

Here δ is defined as the "noise sensitivity." The choice of $10\log_{10}N$ (i.e., dB "whales re 1 whale") as a measure of population change is convenient since we are using dB units to describe ambient noise levels. The term $Q_{indiv} = \partial(S_{dB})/\partial(10\log_{10}N) + (N/f)(\partial f/\partial N)$ measures the change in the acoustic behavior of an individual singer in response to a small fractional increase in the population size around it. For example, whales may increase their source levels slightly with increases in ambient noise level. This "Lombard effect" is incorporated into the Q_{indiv} term.

An interesting consequence of Eq. (3) is that δ (the sensitivity) is relatively independent of S and f, provided that an

individual animal's singing behavior does not change much with a small fractional increase in singer population size [i.e., if the term Q_{indiv} is small compared to the other terms in Eq. (3)]. Stated another way, details about individual whales' acoustic behaviors do not need to be assumed: what is assumed is that the behaviors (whatever they are) change negligibly with a small change in relative population size. The sensitivity term, δ, in Eq. (3) thus becomes dominated by spatial density terms (the dependence of area A on population N) and acoustic propagation factors (the propagation P term). Since propagation parameters can be estimated with knowledge about the ocean floor's geology and the sound speed profile measurements, the only remaining unknown parameters in Eq. (3) include those describing how the species in question is spatially distributed.

Equation (3) can be simplified further by introducing a population density "packing" model. This packing model relates increases in region A with changes in population N. To do this, note that many scenarios of interest in the open ocean can be modeled as a power law, where A is proportional to N^{ν} (i.e., $dA/A = \nu dN/N$) and ν is a fixed constant. Using this expression, Eq. (3) becomes

$$\delta = 1 + Q_{indiv} + \nu\left[\left(\frac{A}{P}\right)\frac{\partial P}{\partial A} - 1\right]. \tag{4}$$

An exploration of Eq. (4) yields two extreme scenarios of how animals may "pack" together: a "constant area" (CA) scenario ($\nu = 0$) and a "constant density" (CD) scenario ($\nu = 1$). Figure 2 illustrates these two extremes.

1. CA scenario ($\nu = 0$)

Under the CA scenario, it is assumed that the region occupied by singers is independent of population size, so that doubling the population would double the singers' spatial density. The "density estimation" approach of line and point transect theories implicitly assumes a constant area scenario, where population density is expected to be proportional to population (Marques *et al.*, 2009; Marques *et al.*, 2013). To simulate this, ν can be set to zero in Eq. (4) to yield

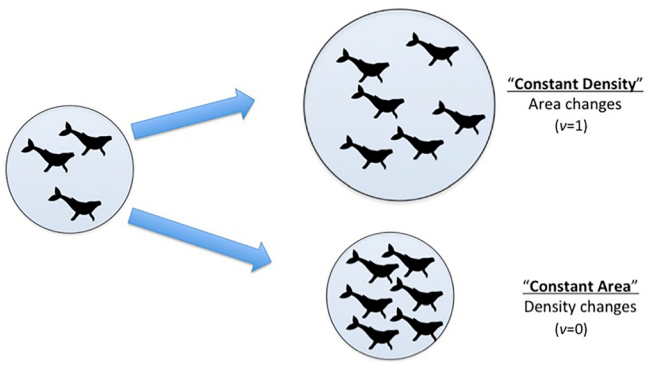

FIG. 2. (Color online) In a CD scenario (top), the area over which whales are singing expands in order to maintain a constant spatial density. In a CA scenario (bottom), the spatial density within that area increases in order to maintain the same the regional size over which the whales are singing.

$$\delta_{CA} = 1 + Q_{indiv}. \tag{5a}$$

Thus, δ, as defined in Eq. (3), should be close to or greater than 1 as long as Q_{indiv} is negligibly small. Equation (5a) is of particular interest to our study because it predicts that δ, the "sensitivity," is independent of not only the propagation environment, but also of the acoustic frequency being measured (that is, unless Q_{indiv} is frequency dependent).

2. CD scenario ($\nu = 1$)

At the other extreme of Eq. (4), singers may space themselves apart evenly. The regional area A becomes proportional to N, and $\nu = 1$. That is, the spatial density of the singers does not change, but the region occupied by singers expands and contracts with respective increases and decreases in the number of singers present. In this case, Eq. (4) becomes

$$\delta_{CD} = Q_{indiv} + \nu\left(\frac{R}{2P}\right)\frac{\partial P}{\partial R} = Q_{indiv} + \frac{1}{2}\left(\frac{\partial \log_{10} P}{\partial \log_{10} R}\right) \tag{5b}$$

where we have assumed a circular sector for A, so that $dA/A = 2dR/R$. Equation (A6) gives an explicit expression for the second term of Eq. (5b) as sums of normal modes.

For high seabed attenuation and large values of R, noise levels become insensitive to population size, so $\delta_{CD} = Q_{indiv}$. The sensitivity becomes higher when both the regional radius R and the seabed attenuation become small. The upper limit of this sensitivity is $Q_{indiv} + 0.5$, which can be seen by taking the Taylor expansion of terms like $(1 - e^{-2\alpha R}) \sim 2\alpha R$ in Eq. (A6). In other words, ambient humpback-generated noise levels increase with the square root of the number of animals (ignoring Q_{indiv}) in the limit of no attenuation. An intuitive explanation for this relationship is that, for a perfectly transparent ocean, the intensity of a single whale will fall off like $1/R$ (cylindrical spreading). The contribution to ambient noise produced by a set of either evenly spaced or randomly spaced whales inside a small annular ring, dR wide, will then be proportional to $(2\pi R)(1/R)dR$, or $2\pi dR$. The total intensity thus becomes proportional to the regional radius R: the square root of the area A, and the square root of the number of evenly spaced animals (N) within that A.

In summary, the KIP model predicts that the ambient noise sensitivities of a CD scenario ($Q_{indiv} < \delta_{CD} < Q_{indiv} + 0.5$) lie below the sensitivities of a CA scenario ($1 + Q_{indiv} < \delta_{CA}$). The reason this sensitivity is lower for the CD scenario is that whenever additional animals arrive, they effectively sing at greater ranges from the sensor, which would not be the case under a CA scenario where all animals would be singing from a predetermined maximum distance. The larger distances in the CD scenario decrease the contribution of an individual singer to the overall ambient noise level being detected at the recorder.

Furthermore, Eq. (5b) shows that, if Q_{indiv} can be neglected, δ_{CD} is a strong function of the propagation environment in terms of both frequency and range R, while δ_{CA} is independent of frequency and details of the propagation environment. Furthermore, if Q_{indiv} can be neglected, δ must

lie between 0 and 1, and v (the packing model parameter) can be inferred from δ. If δ can be empirically measured as a function of frequency, then this theoretical model can be stringently tested. In Sec. II C, we discuss how δ can be empirically measured.

C. Measuring sensitivity (δ) using visual transect surveys

The sensitivity, δ, defined in Eq. (3) can be measured if information about relative population size over time can be determined using separate visual surveys from the acoustic recordings. Since only relative population changes need to be measured [as $d(\log N) = dN/N$], a small line transect survey can be used to estimate δ as long as the following criteria are met.

(a) The area covered by a visual survey is equal to or smaller than the total area A monitored by the hydrophone (assuming that the number of animals present in the visual survey area is proportional to the total population monitored in region A).
(b) The number of animals visually sighted is proportional to the number of singing whales in the larger region; that is, assuming singing whales are a constant fraction of the total demographic population.
(c) The visual survey conditions remain the same throughout the survey (e.g., visibility and effort per unit area), so that raw counts can be used to measure relative changes in population. Thus typical line transect correction factors such as g(0)—the number of animals likely to be right on the transect line—are not required.

Note that assumption (b) allows for an estimate of δ even under a constant density (CD) scenario. One might think that under a CD scenario, repeated visual surveys over the same small area should yield the same number of animals (since the spatial density of singers remains constant). However, a constant spatial density only exists for the particular subset of the population that is singing during a particular moment in time. As behavioral states change over time, we assume humpback whales (including non-singing whales) rotate through different spatial density patterns (alone, in pairs, or in multiple animal competition pods).

If these three conditions are met, then measuring δ becomes straightforward. Changes in raw animal counts made during small visual surveys can be used to estimate the relative fractional changes of the singing population between days, hours, weeks, etc., because then $d(\log N_{survey}) = d(\log N_{singers})$. The advantage of a combined visual and acoustic dataset is that the resulting estimates of δ provide a more stringent test of the KIP model.

As seen above, the magnitude of δ provides insight into how the animals distribute themselves with respect to each other. Neglecting the term Q_{indiv}, if singing animals do not space themselves apart (CA model), then $\delta \sim 1$, independent of the acoustic frequency measured. If animals do space themselves apart (CD model), the noise field becomes less sensitive to changes in population size so that $0 < \delta < 0.5$, and δ will vary with acoustic frequency.

D. Simulations of ambient noise levels (I_{dB}) and sensitivity (δ) from singing males

Here we estimate various model parameters to illustrate some values of the noise intensity (I) and sensitivity (δ) that might be expected from singing humpback whales off Cabo San Lucas, Mexico, assuming a CD scenario. For these simulations, all whales are assumed to have source levels of 155 dB re 1 μPa @ 1 m, with 4 km spacing between the singers. A duty cycle of 65% is used, based on typical time intervals between units as known from song recorded in this region over the past few years as well as previous findings of typical lengths of units and inter-unit intervals (Payne and Payne, 1985; Mednis, 1991). The most egregious assumption is that the spectral density of the entire song is assumed to be constant between 100 Hz and 1 kHz. After exploring our data, it is noted that the received levels of humpback song tended to be dominated by song components with comparably high source levels throughout this bandwidth, so the assumption is largely held. Additionally, the whales are modeled to sing 20 m deep, even though they have been observed to sing both shallower and deeper.

Beyond behavioral assumptions, this model uses a 90-m deep waveguide with a 1500 m/s isovelocity profile, and a receiver placed at 80 m. The ocean lies on top of a 25 m layer of sand that in turn lies on granite bedrock. Sand has a compressional speed of 1650 m/s, density of 1.9 g/cc, and p-wave attenuation of 1.3 dB/wavelength (Hamilton, 1980). Bedrock has respective values of 2700 m/s, 2.3 g/cc, and 0.16 dB/wavelength. As discussed in Appendix A, a sediment layer needs to be included in the model so that the resulting normal modes can approximate the near-field continuous contribution to the ambient noise field. The most unrealistic physical assumption in the model is that the surrounding bathymetry is flat, whereas a sloping bathymetry with finger canyons would be more appropriate off Cabo San Lucas.

Figure 3(a) shows the resulting received ambient noise power spectral density in dB re 1 μPa^2/Hz for the recorder [Eq. (A3)], as a function of both frequency and regional radius R. One sees that for small regions, the noise levels change quite rapidly with regional radius, but the low-frequency components of the noise spectrum (about 200 Hz and below), become relatively fixed as R increases past 15 km. Higher frequency components are still approaching their asymptotic limit as R reaches 50 km. Even though the original source spectrum was flat, we see that the propagation environment favors the lower frequencies: 50 Hz displays a 25 dB higher spectral density than 1 kHz.

Figure 3(b) shows δ_{CD} as a function of frequency and regional radius R, using the analytic formulas in Eq. (5b) and (A6), and setting $Q_{indiv} = 0$. As predicted for small regions, the value of δ_{CD} approaches 0.5, while for large regions and lower frequencies, the value of δ_{CD} approaches 0: noise levels become unaffected by changes in singing population. Due to the effects of acoustic propagation and receiver depth, the sensitivity in our model is greatest at 600 Hz, and least near 350 and 850 Hz. Although not shown here, these bands of minimum and maximum sensitivity shift frequency with receiver depth. The constant-area δ_{CA} scenario is not

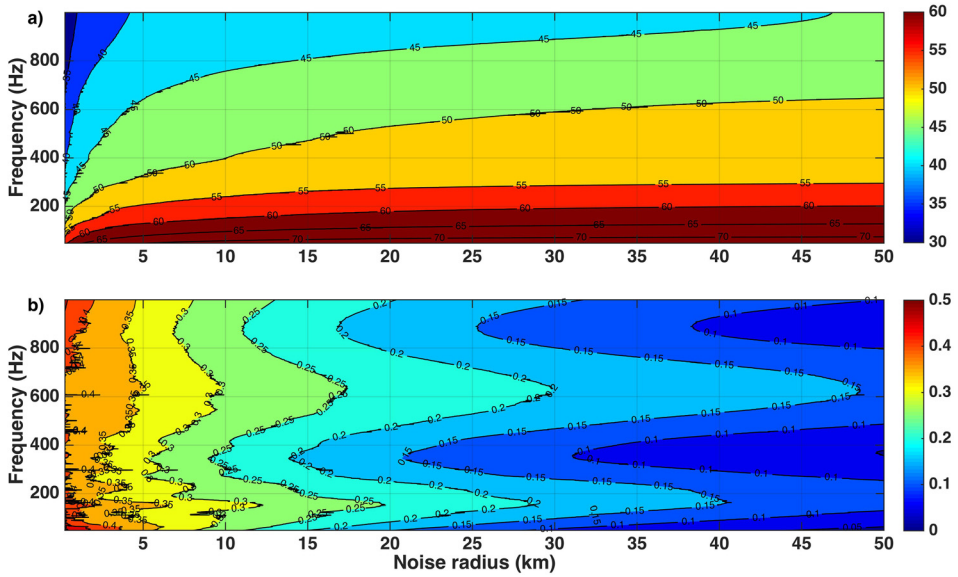

FIG. 3. (Color online) (a) Modeled ambient noise power spectral density (in units of dB re 1 μPa^2/Hz) generated from singing humpback whales in an ocean environment representative of Los Cabos, Mexico, as detected by a recorder deployed 80 m deep in a 90 m deep waveguide. The noise is displayed as a function of frequency and the radius R of the singing region. The power spectral density of the whale song was assumed to be a constant value of 125 dB re 1 μPa^2/Hz between 100 and 1000 Hz (total source intensity of 155 dB re 1 μPa). No additional ambient noise sources are included in the model, so the low levels shown for high frequencies and small values of R may be masked by other ambient noise sources in a real environment. (b) Modeled noise sensitivity δ as a function of frequency and regional radius R for a CD case, computed from Eq. (5b) and (A6), and neglecting Q_{indiv}. The sensitivity is a unitless value that can range from 0 to over 1.

plotted, as it would simply be 1 for all regions and for all frequencies.

Figure 4 displays the ambient noise intensity modeled by integrating the power spectral density in Fig. 3(a) over a set of 50 Hz bandwidths, with five center frequencies between 125 and 925 Hz. A 50 Hz bandwidth was selected because the humpback source level power spectral density (constructed across an entire 20–30 min song duration) is (1) relatively constant over any given 50 Hz bandwidth, and (2) most song units span at least 50 Hz. Appendix B shows that sensitivities estimated from narrowband-integrated ambient noise intensities are still independent of source level and duty cycle. Figure 4(f) differs from the other subplots in that it shows the broadband ambient noise intensity integrated between 100 and 1000 Hz, to give some sense of what the model predictions would be for broadband measurements. For each bandwidth, a linear fit to the ambient noise level vs regional radius yields estimates of δ_{CD} that can be compared

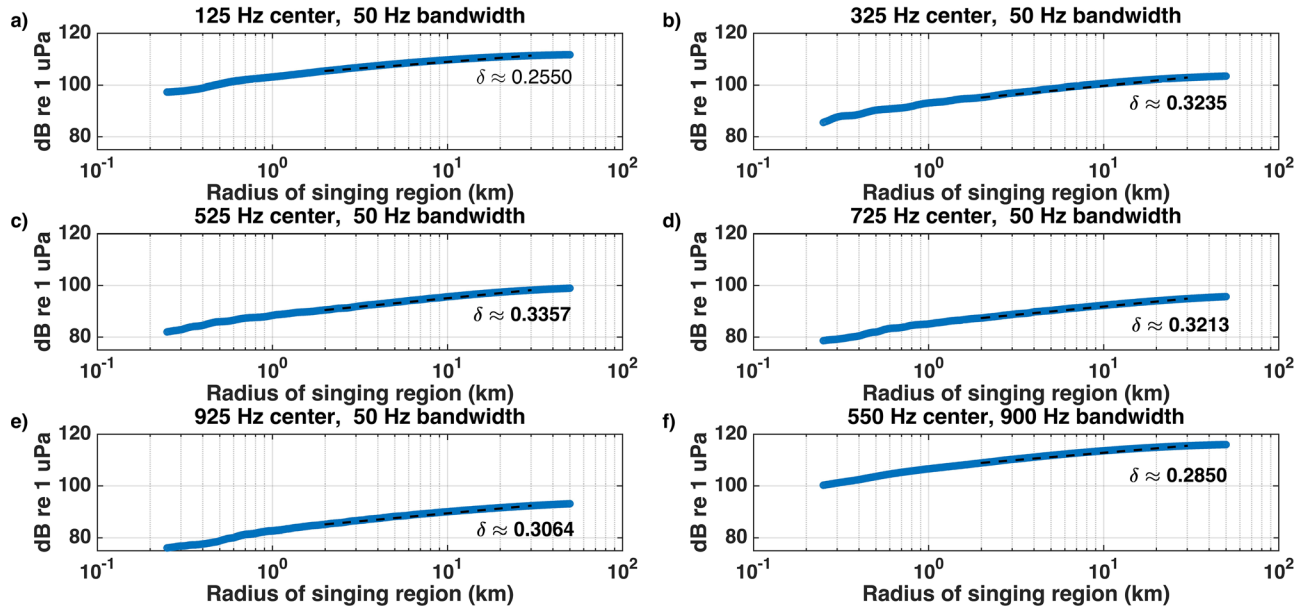

FIG. 4. (Color online) Model of humpback whale ambient noise intensity generated over 50 Hz bandwidths, as a function of singing region radius R, using parameters identical to Fig. 3. Values of an "empirical" δ_{CD} are shown, estimated by a linear fit (dashed line) between 2 and 20 km, and then using Eq. (5b). Center frequencies of the bandwidth samples are (a) 125 Hz, (b) 325 Hz, (c) 525 Hz, (d) 725 Hz, and (e) 925 Hz. Subplot (f) shows a noise estimate integrated between 100 and 1000 Hz and assumes a flat song spectrum.

to empirical data later, as the linear fit mimics the fit of a generalized linear model to the data. The rest of this paper discusses how empirical estimates of δ were produced from field data, for comparison with the values shown in Fig. 4.

III. METHODS

A. Study location

Geographically speaking, "Los Cabos" (Fig. 5) denotes a collection of capes around the tip of Mexico's Baja peninsula. Cabo San Lucas lies on the southwestern-most tip of the Los Cabos region and boasts a large marina primarily used by whale-watching and sport-fishing companies. Boat traffic tends to decrease eastward (from Punta Ballena to Punta Gorda to Cerros Colorados) with distance from this marina.

A subset of the Central North Pacific humpback whale stock breeds off Los Cabos over the boreal winter months, typically from late January to early April (Calambokidis *et al.*, 2008; Jiménez-López, 2006). From past visual survey research, it is known that humpback whale density tends to increase eastward from Punta Gorda to Cabo Pulmo (Jiménez-López, 2006). This is the opposite trend of boat traffic. In the future, a sanctuary at Cabo Pulmo may extend into the Los Cabos region (Dedina, 2014).

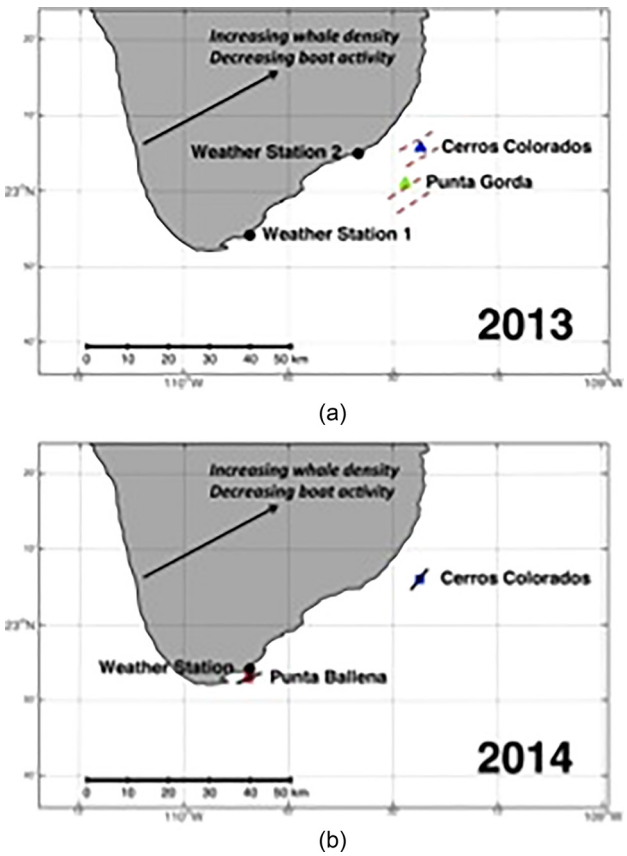

FIG. 5. (Color online) Positions of passive acoustic recorders and visual transects during two breeding seasons off Los Cabos. Visual transects were conducted at all sites for both years, but only transects associated with successful recording sites are shown here. Transect lines were always 10 km long and spaced 4 km apart (causing lines to be centered over Cerros Colorados, but not over Punta Gorda in 2013). In 2013 [(a)], two track lines were surveyed; in 2014 [(b)] only a single track line was surveyed.

There are several reasons why this region provides an opportune location to test the KIP model. First, the local bathymetry allows acoustic recorders to be placed at nearly the same depth, in the same expected propagation environment, and the same distance from shore at several sites throughout the area. Second, visual surveys of the local humpback population have been extensively conducted by Laboratorio Marinos Mamíferos at the Universidad Autónoma de Baja California Sur (UABCS) in La Paz throughout the past couple of decades. UABCS has found that humpback whales stay close enough to shore to feasibly perform boat-based visual line transect surveys at multiple sites between Punta Ballena and Cerros Colorados over the course of a single day (Jiménez-López, 2006). Third, the spatial population gradient mentioned above means the number of whales between locations differs substantially, even though these locations are close enough to be surveyed in a single day.

B. Passive acoustic locations

Acoustic recorders were deployed along the Los Cabos coast for approximately two months during both 2013 and 2014. For the remainder of this paper, specific deployment locations will be called "sites." Sites were chosen based on past knowledge of both relative boat activity and gradients in humpback whale density. An attempt was made to place recorders equidistant from shore, as long as bathymetry allowed them to sit at nearly the same targeted depth of 90 m. Acoustic recorders were also placed close enough so all sites could be easily traversed by the same whale, increasing the likelihood that all three sites would monitor the same whale population. Conversely, there was sufficient spacing between recorders to prevent their effective recording radii from overlapping, reducing the chance of a singing whale from being recorded concurrently at more than one site.

In 2013 the sites included Punta Ballena (high boat activity, low whale concentration), Punta Gorda (moderate boat activity, medium whale concentration), and Cerros Colorados (low boat activity, high whale concentration). In 2014 it was determined that Punta Gorda was too close to Cerros Colorados for a true representation of an area with moderate boat traffic, so a site farther West at Punta Palmilla replaced it. Punta Ballena and Cerros Colorados, however, were still monitored in 2014. Figure 5 maps locations for both years

C. Passive acoustic equipment and deployment procedures

The same bottom-mounted recorders described by Ponce *et al.* (2012) collected acoustic data. Although duty cycle differed by year, the sampling rate was 6.125 kHz for both years at all sites. In 2013, data were recorded for thirty minutes every hour (50% duty cycle), but in 2014 data were recorded continuously (except for a few hours every two days, when data were written to a hard disk). The hydrophones used for both years were HTI-96-MIN (High Tech

Inc.) with a −171 dB re 1 V/μPa sensitivity. The recorders were combined with handmade anchors (four burlap bags filled with gravel in 2013; four 25 kg cement blocks in 2014), a Sub Sea Sonics A-60-E acoustic release, and two 714 Trawlworks subsurface buoys, using both manila and nylon line to create an assembly. HOBOware Tidbits and inclinometers were also attached to the assemblies to collect temperature and tilt data. The final assembly placed the hydrophone 10 m above the ocean floor, consistent with the simulations in Sec. II B. Table I lists the dates, coordinates, and depths for all acoustic recorder sites. Note that depths are bottom depths, but the hydrophone actually sat 10 m above the ocean bottom.

D. Visual transect protocol and procedures

Visual transects using standard line transect protocols were performed both years using the panga *Yubarta*, but with slightly different track lines—an important factor that was considered in subsequent statistical analysis. In 2013, two transect lines were traversed at 4 km spacing from each other, starting 2 km from the coast (since the visual range from the *Yubarta* was 2 km). This centered track lines above Cerros Colorados, but caused them to be off-center above Punta Gorda. For better efficiency in 2014, the track lines were reduced to a single line that passed over the top of each acoustic recorder (Fig. 5).

All other protocols remained the same for both years: the *Yubarta* was driven at 5 knots along the 10 km-long transect lines that ran parallel to the coast. The visual observers scanned the forward quadrant on their respective sides of the panga and, upon sighting a whale, reported the group type, number of animals, and distance from the *Yubarta* to an onboard scribe. To decrease chances of resighting animals, whales were only counted when their sighted location was orthogonal ("off the beam") to the transect line.

Environmental conditions were observed before each survey. These included water temperature, Beaufort level, cloud cover, wind direction, visibility, swell height, and glare. Each transect line took roughly 1 h to complete. Visual surveys were performed only in seas at Beaufort levels 0 and 1, so the visual detection range (and detection function) was consistent across the surveys, fulfilling one of the requirements listed in Sec. II C.

E. Statistical analysis

1. Visual data analysis

Several types of analyses of the visual surveys were used to tabulate sighted whales. Multiple possibilities existed for measuring the relative singing population: (1) counting only whales that were sighted alone, since singers tend not to sing in groups ("solo"), (2) counting all sighted whales, excluding mother/calf pairs ("no m/c"), and (3) counting all sighted whales, including mother/calf pairs ("all"). Ideally, only male whales should be counted, since only males sing, but since whales could not be sexed, all three options could easily include females. We thus assume that males comprise a consistent fraction of the sighted population, as discussed in Sec. II C.

2. Acoustic data analysis

The acoustic noise data analysis required several steps. First, the raw binary acoustic data were downloaded from the recorders and converted into pressure units, and the frequency spectrum was corrected for the hydrophone sensitivities. Short-term power spectral densities (PSDs) in dB re 1 μPa^2/Hz up to 3.125 kHz were estimated to 24-Hz resolution by averaging the FFT snapshots (overlapped 50%) over one minute. Subsequent calculations were restricted to a 100–1000 Hz bandwidth because humpback whale song at these locations mainly resided between these frequencies (see Fig. 1). Nine 50-Hz bands within that bandwidth were also computed: 100–150, 200–250, 300–350, 400–450, 500–550, 600–650, 700–750, 800–850, and 900–950 Hz. Next, 1-min averaged PSDs were integrated over these bandwidth estimates to compute the average acoustic intensity each minute. Percentile distributions of these intensities were then generated over one-hour intervals, and the 1st, 10th–90th (in tenths), and 99th percentiles were extracted for further analysis. As a result, a given percentile could be plotted against time with hourly resolution for all sites over both years. Cyclical and secular fluctuations were easily spotted in these plots (see Fig. 7 for an example plot).

To determine whether a diel song cycle was occurring in Los Cabos, as is the case at Hawaii and other breeding grounds (Au *et al.*, 2000; Cholewiak, 2008; and Sousa-Lima and Clark, 2008), the PSD percentile histograms were averaged and

TABLE I. A listing of the time frames, depths, and locations of all autonomous acoustic recorders analyzed in this report.

2013	Punta Ballena	Punta Gorda	Cerros Colorados
Lat/Long	n/a	23.017 N, 109.472 W	23.094 N, 109.437 W
Depth		105 m	106 m
Acoustic Survey		Feb 8–Apr 1	Feb 8–Apr 1
Visual Surveys		Feb 18, 19, 24	Feb 18, 24
		Mar 7, 18, 21, 27	Mar 6, 18, 21
2014			
Lat/Long	22.884 N, 109.843 W	n/a	23.102 N, 109.437 W
Depth	92 m		95 m
Acoustic Survey	Feb 7–Mar 26		Feb 6–Mar 26
Visual Surveys	Feb 13, 15, 22, 25		Feb 11, 15, 22
	Mar 1, 4, 13, 20		Mar 1, 5, 12, 20

plotted as a function of the hour of day. For example, all the intensity values from the 50th percentile computed between 0100 and 0200 from each day at a given site were averaged, and then repeated for all twenty-three subsequent hours. A strong diel cycle did exist, whereby whales off Los Cabos tended to sing most actively near midnight and tapered off at sunrise. This phenomenon was accounted for when comparing visual transect data to the acoustic data.

Figure 6 illustrates five acoustic metrics that were used in an attempt to remove this diel effect. All of the acoustic metrics were measured using the 50th percentile from the one-hour "noise" samples. The metrics included (A) the peak sound intensity from the night before a visual survey, (B) the peak sound intensity from the night after a visual survey, (C) the sound intensity from the hour concurrent with the visual survey, (D) the average of the peak intensities from the nights before and after a visual survey, and (E) the average of the peak-to-trough intensities from the nights on either side of a visual survey. This last metric (E) measures the extent (or strength) of the diel cycle and assumes that the daytime troughs are the contribution of non-whale noise sources to the environment. While metric (C) might seem to be an obvious choice, it is contaminated by boat engine noise from *Yubarta* during the visual survey effort.

3. Estimating the sensitivity δ

The final step in data analysis was to combine the various visual counts and acoustic metrics for each frequency band via a generalized linear model (GLM) to determine which pairing had the most significant fit, and then measure the δ (sensitivity) of that combination.

To estimate δ [Eq. (3)] from the data, the following GLM was used:

$$I_{dB} = \beta + \delta(10\log_{10}N) + \gamma[Year], \quad (6)$$

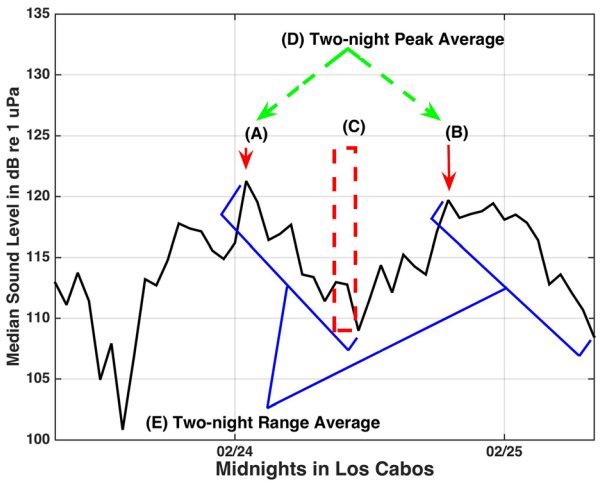

FIG. 6. (Color online) The five sound metrics used were the hourly average of the 50th percentile of the sound level at (A) the peak hour the night before a survey, (B) the peak hour the night after a survey, (C) the hour concurrent with a visual survey, (D) the mean of the peaks from the nights before and after a survey, and (E) the mean of the maximum dB variation of the nights before and after a survey.

where I_{dB} is one of the acoustic metrics described in Sec. III E 2, expressed in dB, and N represents one of the visual counts discussed in Sec. III E 1. β (dB) is the y-intercept of the fitted line, and γ is the coefficient of a categorical variable *Year* that accounts for differences in methodology between years. The specific methodological differences include (1) recording duty cycles (50% in 2013; 100% in 2014), (2) track lines (two in 2013; one in 2014), (3) site locations (Punta Gorda and Cerros Colorados in 2013; Punta Ballena and Cerros Colorados in 2014), (4) song unit changes (humpback whales can change their song every two to three weeks (Norris *et al.*, 2000), and (5) hydrophone depths (104 and 105 m in 2013, 92 and 95 m in 2014).

The predictor coefficient of the multiple regression (δ) can be interpreted as the slope of the line relating the base-10 logarithm of the visual count with the dB value of the acoustic metric after the visual counts were corrected for year. This coefficient is an empirical estimate of the sensitivity δ. The corresponding values from the model were obtained by computing the linear slopes from the subplots in Fig. 4, between regional radii that were expected to be the minimum and maximum encountered over the course of a season. These values were estimated to be 2 and 20 km, respectively.

All combinations of the five acoustic metrics and three visual counts were run through generalized linear model scripts in the Matlab statistics toolbox. The R^2, test statistics, p-values, and all coefficients were tabulated for all combinations and compared to find the best R^2 value that was also significant to a p-value of 0.05. The visual count and acoustic metric pairing that yielded the highest R^2 values with the lowest p-values (as presented in Table IV) were then explored with multiple model specifications for the best Akaiki Information Criterion (AIC) value.

IV. RESULTS

A. Visual surveys

The cumulative visual survey results are presented in Table II in terms of the three visual counts. These counts are used to provide an illustration of seasonal whale densities. For example, over the course of 2013 observers noted 22 "solo" whales, 47 "no-m/c" whales, and 51 "all" whales at Punta Gorda. These counts are consistent with the expectation from Jiménez-López's (2006) master's thesis that humpback whale density increases eastward from Cabo San Lucas. Also note that more whales were detected in the Los Cabos area in 2013 than in 2014.

TABLE II. The total number of all whales counted, all whales excluding mother/calves, and solos counted at each site for each year.

Year	Punta Ballena	Punta Gorda	Cerros Colorados
	"all"/"no-m/c"/"solos"	"all"/"no-m/c"/"solos"	"all"/"no-m/c"/"solos"
2013	n/a	51/47/22	142/136/58
2014	50/46/26	n/a	97/85/34

B. Noise measurements

In 2013 an electronic malfunction in the recorder at Punta Ballena caused it to stop logging after only five days. The Punta Gorda and Cerros Colorados datasets lasted from February 8, 2013 to April 1, 2013. In 2014, recorders at Punta Ballena and Cerros Colorados successfully collected data from February 7 to March 28, but the recorder at Punta Palmilla broke free and drifted 13 km Southwest until it slipped into a finger canyon and was never recovered.

Figure 7 displays the 50th percentile of the ambient noise levels between 300–350 Hz, computed for each hour during the 2013 recording season at Cerros Colorados. Clearly, the noise intensity over this bandwidth can vary greatly (up to 15 dB or more) on a daily basis. From Eq. (2), a 15 dB daily noise shift corresponds to fluctuations in N numbers by a multiplicative factor of 30. When comparing sites from the same season, Punta Gorda (moderate boat traffic) and Cerros Colorados (low boat traffic) in 2013 are more similar than Punta Ballena (high boat traffic) and Cerros Colorados (low boat traffic) in 2014. In 2013, the average 50th percentile values were 104 dB re 1 μPa at Cerros Colorados and 100 dB re 1 μPa at Punta Gorda. The average 50th percentile values for 2014 were 101 dB re 1 μPa at Cerros Colorados and 96 dB re 1 μPa at Punta Ballena. Since Cerros Colorados was the only site recorded over both years, we find that the same midnight-peaking trend exists at both years, but the average 50th percentile value for 2014 was 3 dB less than in 2013 (Fig. 7).

Figure 7 illustrates that nightly peaks in sound intensity at the 50th percentile tend to fall between about 102–107 dB re 1 μPa in the 300–350 Hz bandwidth. (The peaks are more consistently about 120 dB re 1 μPa in the 100–1000 Hz bandwidth.) Recall that the simulations in Fig. 4(f), which assumed whale source levels of 155 dB re 1 μPa @ 1 m and animal separations of 4 km, predicted a received level of 100 dB re 1 μPa for R = 10 km for the 300–350 Hz bandwidth. Some of the nightly 50th percentile peaks, especially near the end of the season, do fall near 100 dB re 1 μPa.

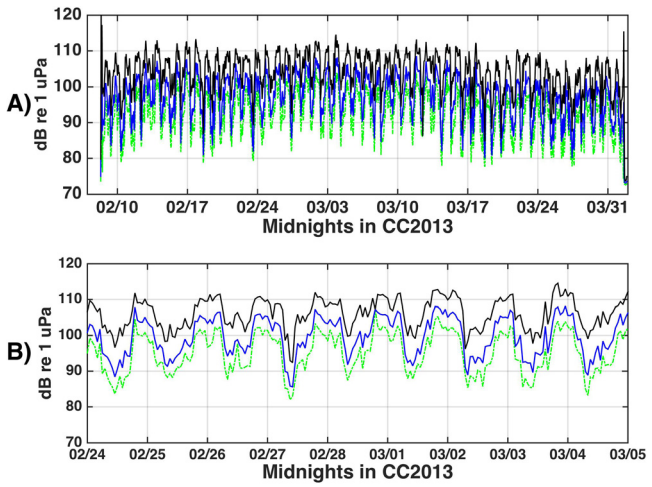

FIG. 7. (Color online) (a) Plots of the 10th, median, and 90th percentiles of the noise intensity computed between 300 and 350 Hz for every hour across the entire 2013 recording season at Cerros Colorados. (b) An expansion of time scale in (a) to show nine days in detail. A diel cycle is clearly visible, with a peak:trough dynamic range of 10–15 dB.

C. GLM results

The GLM was applied to several bandwidths. After calculating δ for all visual counts and acoustic metric combinations for both combined and separated years, the R^2 values with significant p-values were compared. The model [sound $\sim 1 + \text{year} + \text{count}$] using only linear terms in the two predictor variables performed better than (had lower AIC values than) using an interaction term between the two. AICs were also higher for using quadratic terms in the models ([sound $\sim 1 + \text{year} + \text{count} + \text{count}^2$] and [sound $\sim 1 + \text{year} + \text{count}^2$]). Therefore, the simplest linear model using acoustic metric D and visual count "all" best explained our empirical data.

Figure 8 shows dB noise vs the logarithm of the transect counts (adjusted for the effect of year) along with the best-fit lines for each year. It also shows the predicted values, the slope (δ) of the combined years, and the slope's 95% confidence bounds. The estimated δ value for the 300–350 Hz bandwidth was 0.436 ± 0.114 dB re 1 μPa (p-value $= 6.12 \times 10^{-4}$, t-test statistic $= 3.81$), a value that falls within the theoretical range (0 to 0.5) of the CD scenario, and is too low for the CA scenario.

The low p-value indicates that we can reject the null hypothesis that the acoustic metric did not differ statistically from a constant (i.e., the probability that the sensitivity coefficient is zero). Table III summarizes the results for all bandwidths using the acoustic metric D, the two-night average, and the "all" whales visual count, since this pairing consistently yielded the best R^2 values. Note that not all bandwidths were affected equally by year, but did fall within reasonable (1–6 dB) differences considering the five methodological changes between 2013 and 2014.

As presented in Table III, the best R^2 value was found between 300–350 Hz (0.60) using acoustic metric D (averaged peak intensity from night before and after the survey) and the "all whales" count. Table IV is an expansion of Table III for all acoustic and visual metrics. The "no m/c" visual count yielded nearly equivalent results. For the remainder of this section, we focus on the results of this 300–350 Hz bandwidth. β, or the y-intercept, was 105 ± 1.10 dB re 1 μPa. γ was 5.80 ± 0.93 dB re 1 μPa: that is, for a given value of $10\log N$, a roughly 5 to 7 dB difference in background noise levels existed between years (p-value $= 6.73 \times 10^{-7}$, test statistic $= 6.21$). The 300–350 Hz bandwidth had the largest γ. Other bandwidths exhibited smaller differences between years (1.09 to 4.43 dB). The three methodological differences between acoustic and visual data collection between 2013 and 2014 are contributing factors to the non-zero value of γ; the possibility that changes in song structure between years may also affect γ will be discussed later.

Figure 9 shows histograms and normal probabilities of the residuals of the GLMs for the fit in Fig. 8. The residuals approximately have Gaussian distribution, except possibly at the tails, indicating that the choice of a Gaussian-based GLM is appropriate.

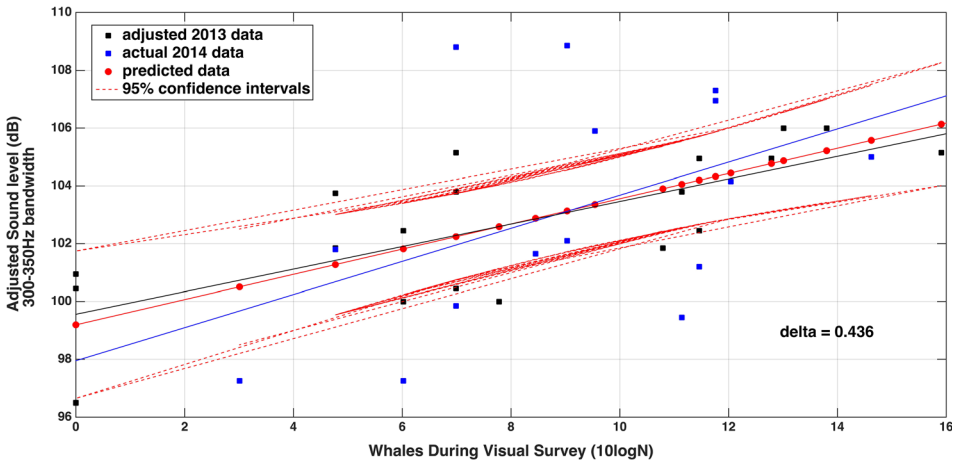

FIG. 8. (Color online) Plot of ambient background noise level (acoustic metric D) in the 300–350 Hz bandwidth vs the base-10 logarithm of the number of all whales sighted during concurrent visual transects. Shown by squares in two hues are the adjusted data points and best-fit lines for both years (2013 darker and 2014 lighter). The slope of the GLM-fitted values (δ), which corresponds to the population sensitivity defined in Eq. (3), is designated by circles. Data have been weighted by year because 2013 tended to be 5–7 dB higher overall than 2014. 95% confidence bounds are shown in dotted lines. The slope of the combined-year data ($\delta = 0.436$) is displayed as text.

D. Comparing measured sensitivity with analytic model predictions vs bandwidth

Figure 10 shows δ for the Sec. II D. constant-density scenario [Eq. (6)], a singing region 20 km radius, for nine 50-Hz bandwidths discussed in Sec. III. In addition, the linear least-squares estimate of δ (average sensitivity between 2 and 20 km) is also plotted for each bandwidth (e.g., Fig. 4). Also shown are the GLM δ values from Table III, and their standard errors. As illustrated, all of the actual δ values fall between 0 and 0.5. Even when accounting for standard errors, the CD scenario (where $0 < \delta < 0.5$) is a much better fit to the actual data than the CA scenario ($\delta \sim 1$). Stated another way, Fig. 10 suggests that singing humpback whales tend to maintain a relatively consistent distance between individuals as additional whales arrive.

The observed sensitivities also obtain their maximum and minimum values at the same bandwidths as the modeled values. For example, both observed and modeled sensitivities are minimal between 300–400 Hz and between 800–900 Hz. Even though the observed δ values fall between 0 and 0.5, they all lie above the analytically expected values for a strict CD ($v = 1$) case. Section V lists three possible interpretations for this mismatch between the measurement and the CD simulation.

V. DISCUSSION

A. Interpretation of the best acoustic metric and visual count

Considering several acoustic metrics and visual counts, the best ones for the generalized linear model (highest relative R^2 value with significant p-values at the 0.05 level) were, respectively, an average sound intensity of the peaks the night before and after a visual survey (metric D), and either "all whales" or "no m/c." It makes sense that the average nightly peak in sound intensity is a representative metric if we assume that the same whales spotted during the visual survey were representative of the whales that sang in the vicinity of that recorder during the nights before and after they were counted.

An advantage to using nightly peaks (instead of daytime levels) is that it avoids contamination from boat engines since vessel activity is very low, and likely nonexistent, between dusk and dawn. A second advantage comes from measuring the sound intensity peaks each night instead of limiting measurements to the same hour each night, presumably compensating for any lunar effects that humpback whales may have responded to over the two fortnights that visual surveys took place (Sousa-Lima and Clark, 2008).

TABLE III. Best-fit coefficients for GLM in Eq. (6), for different noise bandwidths, combining both years of data. The predictor variables with the highest R^2 were "all" whales and a categorical year with no interaction term. Acoustic metric D (Fig. 5) yielded the best-fit response variable. The year coefficient quantifies the difference in sound intensity between 2013 and 2014. The intercept projects the sound intensity of the ambient environment if no singing activity was occurring based on the best fit line through the year-adjusted data.

Bandwidth	δ slope (SD)	R^2	p-value	Year γ (SD)	Intercept (SD)
100–150 Hz	0.365 (± 0.090)	0.38	3.11×10^{-4}	1.63 (± 0.73) dB	104 (± 0.86) dB
300–350 Hz	0.436 (± 0.114)	0.60	6.12×10^{-4}	5.80 (± 0.93) dB	105 (± 1.10) dB
500–550 Hz	0.518 (± 0.140)	0.31	8.15×10^{-4}	1.09 (± 1.14) dB	92 (± 1.34) dB
700–750 Hz	0.524 (± 0.144)	0.43	9.70×10^{-4}	4.43 (± 1.17) dB	89 (± 1.38) dB
900–950 Hz	0.445 (± 0.120)	0.36	8.19×10^{-4}	2.38 (± 0.98) dB	85 (± 1.15) dB
100–1000 Hz	0.383 (± 0.087)	0.42	1.24×10^{-4}	1.74 (± 0.71) dB	115 (± 0.84) dB

TABLE IV. Best-fit coefficient (δ) and R^2 values for the GLM in Eq. (6), for different combinations of visual counts and acoustic metrics using the 100–1000 Hz bandwidth. Like Table III, this combines both years of data. The predictor variables with the highest R^2 were "all" whales visual count with the nightly average (D) acoustic metric. Based on these results, this predictor variable pairing was further tested for the highest R^2 values across multiple bandwidths (Table III).

Acoustic metric	Visual count	R^2	p-value	δ slope (SD)	Intercept (SD)
A	All	0.33	1.70×10^{-3}	0.45 (± 0.13) dB	114 (± 1.26) dB
	No-m/c	0.31	2.70×10^{-3}	0.45 (± 0.14) dB	114 (± 1.30) dB
	Solos	0.14	1.89×10^{-1}	0.25 (± 0.18) dB	117 (± 1.24) dB
B	All	0.26	3.00×10^{-3}	0.31 (± 0.10) dB	115 (± 0.93) dB
	No-m/c	0.25	3.50×10^{-3}	0.32 (± 0.10) dB	115 (± 0.95) dB
	Solos	0.14	4.99×10^{-2}	0.26 (± 0.12) dB	117 (± 0.87) dB
C	All	0.14	6.48×10^{-2}	0.31 (± 0.16) dB	105 (± 1.54) dB
	No-m/c	0.15	5.64×10^{-2}	0.38 (± 0.09) dB	105 (± 1.55) dB
	Solos	0.28	3.70×10^{-3}	0.38 (± 0.09) dB	105 (± 1.22) dB
D	All	0.42	$\ll 10^{-3}$	0.25 (± 0.13) dB	115 (± 0.84) dB
	No-m/c	0.40	$\ll 10^{-3}$	2.38 (± 0.98) dB	115 (± 0.86) dB
	Solos	0.18	5.36×10^{-2}	1.74 (± 0.71) dB	117 (± 0.85) dB
E	All	0.42	1.25×10^{-1}	1.09 (± 1.14) dB	30 (± 12.40) dB
	No-m/c	0.41	1.75×10^{-1}	4.43 (± 1.17) dB	29 (± 12.68) dB
	Solos	0.38	5.60×10^{-1}	2.38 (± 0.98) dB	19 (± 10.10) dB

As for visual counts, "all" whales and "no m/c" in the model provided similar results. This supports the assumption in Sec. II C that the numbers of singing males and mother/calf pairs are constant fractions of the total population. Even the best visual team cannot sex all whales spotted. Using "all" as the visual count considers all potential singers at each site in case; for example, if a pair of males was falsely classified as a mother and calf or a single male was in fact a female.

B. Explaining the difference between simulated and measured noise sensitivity

The simulated sound intensity values over a broad bandwidth [Fig. 4(f) at large R] fall very close to the nightly peaks of sound intensity (Fig. 7). Actual data showed a fairly consistent 105 dB re 1 μPa sound level for the 300–350 Hz bandwidth at the 50th percentile. Figure 10 shows that the measured δ values fell more within the permissible δ values for the CD scenario instead of the CA scenario. Furthermore, the measured sensitivities showed the same general dependence on frequency as the CD simulations. These results suggest that humpback whales generally space themselves equidistantly from each other while singing, and that the region covered by singing whales expands as more whales enter the area. However, the actual δ values were higher than what was expected from the modeled CD scenario. Some insights into why this discrepancy exists include the following.

(1) Animals may pack a little tighter when the population grows by acquiescing to the higher numbers and tolerating a slightly closer spacing. If they behaviorally reduced their distances between each other slightly over the same area, then modeling an intermediate scenario between the extreme CD and CA scenarios can explain our empirical results. In order for the model to reproduce the empirical GLM model values, a packing coefficient value of $v = 0.7$ must be assumed instead of 1, increasing the modeled sensitivity at 500 Hz from 0.35 to 0.5. A value of 0.7 translates into a reduction in spacing by about 20% as the singing population doubles.

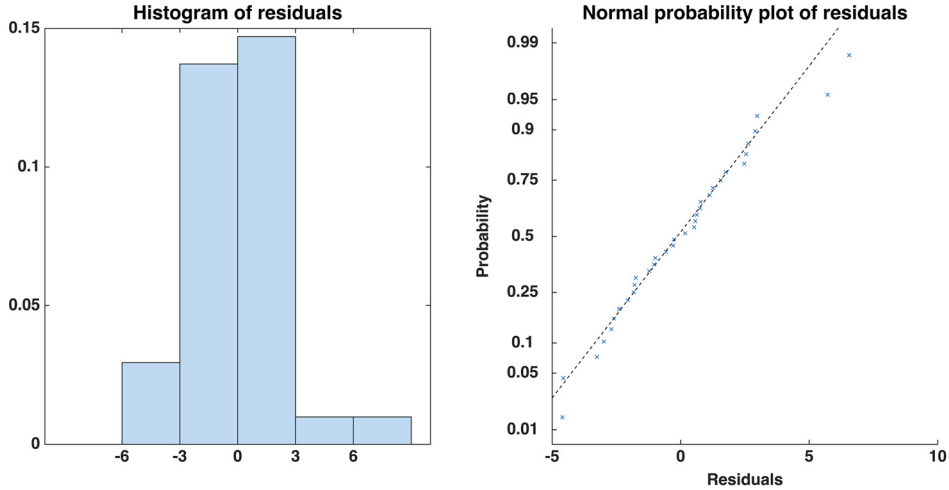

FIG. 9. (Color online) The distributions of residuals (left; observed minus fitted values) and cumulative distribution functions of residuals (right) from the GLM for the 300–350 Hz bandwidth.

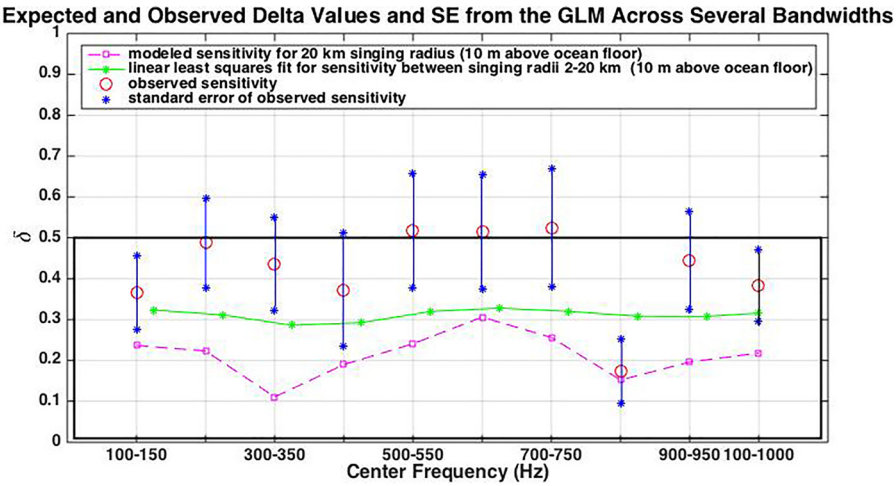

FIG. 10. (Color online) The observed values (open circles) of δ for nine different bandwidths and their standard errors (starred lines) compared with theoretical values (solid and dashed curves) for a constant-density scenario. The dashed curve represents the sensitivity evaluated at a fixed singing radius of 20 km. The solid curve reproduces the values of δ obtained from the slopes of the dashed lines shown in Fig. 4, which effectively estimates the average sensitivity measured from a population of singers that expands its region from 2 to 20 km between measurement periods. Observed values are obtained directly from the GLM using all counted whales and acoustic metric D. The solid box represents theoretically permissible values of δ for a constant-density model, where $Q_{indiv} = 0$. A constant area scenario would yield values of 1 or larger.

(2) Animals may alter their individual acoustic behavior (Q) in one or a mix of the following three ways: (A) by increasing their source level when other animals are present, (B) by "speeding up" the "tempo" between their units, or (C) by using units that have smaller inter-unit intervals. Any of these behavioral changes would make Q_{indiv} in Eqs. (3) and (4) nonzero. For example, the results suggest that if Q_{indiv} were 0.15 then the constant density simulation would match the observed results at 500 Hz. This value of Q_{indiv} could be generated if humpback whales increased their source level by 0.3 dB (increased their output intensity by 7%) if the population doubles.
(3) The bathymetry of Los Cabos is not actually flat as assumed in the model.
(4) The male/female mixture may change when more females are present. More whales counted during a survey may have included more females and, as a result, the nearby males may have been singing differently if it coincided with more females since the effect of ovulation on singing is not well-known (Nishiwaki, 1959; Tyack, 1981; Baker and Herman, 1984; Darling and Bérubé, 2001).
(5) Animals may not be randomly distributed throughout area A, and therefore individual singers may not contribute equally to the overall noise levels recorded. However, Appendix B discusses how a simple linear spatial gradient in singer density would not affect these conclusions.

The discrepancy between the observed and modeled CD values may arise from a mix of all of these factors. Regardless, our results (Fig. 10) are consistent with the hypothesis that humpback whales in Los Cabos space themselves according to a CD scenario more so than to a CA scenario. This prediction is consistent with published observations of how singing humpback whales separate themselves while singing (Winn and Winn, 1978; Tyack, 1981; Frankel *et al.*, 1995). In addition, consistency of the magnitude and frequency-dependence of the sensitivity between measured and modeled values (Fig. 10) supports the fundamental assumptions of the KIP model.

VI. CONCLUSION

This paper presents an applied use for theoretical waveguide models. The main caveat is that the vocalizing species of interest produces nearly continuous sound in a specific bandwidth. In essence, the goals of this technique was to model an expected δ value for an area with known bathymetry and sound speed profile, and then compare it to a GLM using empirical data so δ could be appropriately adjusted and interpreted. This theoretical model showed that changes in ambient noise levels with respect to fractional changes in singer population are relatively unaffected by the source level distributions and song spectra of individual humpback whales, but δ does depend on frequency and on how the singers' spatial density changes with population size. As a result of comparing the theoretical model with the GLM, it is suggested that humpback whales tend to maintain relatively constant spacing between one another while singing. The small discrepancies between the two models are likely due to individual whales singing slightly "louder" or with a faster duty cycle when other singers are nearby, or that they cluster a bit more tightly as the singing population increases.

The techniques discussed here are not restricted to just humpback whales, but could be applied to other ambient noise situations that are dominated by bioacoustic signals. Depending upon the season, blue, pygmy blue, and fin whales may be good future candidates for testing and applying these models (McDonald and Fox, 1999; Gavrilov and McCauley, 2013) and would be valuable for reserve management personnel or scientists who are interested in quantifying a general increase or decrease in the relative abundance of animals.

ACKNOWLEDGMENTS

This project would not have been possible without the extensive dedication of our visual team from UABCS in La Paz, Mexico. First and foremost: a huge thanks to Juan Carlos Salinas as our panga-driving extraordinaire with his general masonry know-how. Next, thank you to photo ID and humpback whale experts P.M.-L. and M.E.J.-L. If not for their knowledge, passion, patience with certain native English-speakers, and a beloved dusty hatchback, fieldwork would have actually felt like work. Others from UABCS and SIO who have helped include Hiram Rosalez-Nanduca, Carlos López-Montalvo, Lorena Viloria, Jit Sarkar, Melania Guerra, Ludovic Tenorio-Halle, Romina Carnero-Huaman, and Cedric Arissdakessian. Robert Glatts built the acoustic recorders and David Brem made certain that the acoustic releases were easy to operate. Thank you also to Garret Eaton, Art Taylor, and Celia Condit for their assistance in making sure that all gear arrived at its desired destinations. The Ocean Foundation funded this work.

NOMENCLATURE

A	Area of the noise-producing region that surrounds the hydrophone
α	Medium attenuation coefficient
α_m	Imaginary part of the modal horizontal wavenumber
β	The y-intercept of the fitted line in the GLM
θ	Azimuth of the singing whale from the sensor (recorder)
δ	"Noise sensitivity"
δ_{CA}	The noise sensitivity under a "constant area" scenario
δ_{CD}	The noise sensitivity under a "constant density" scenario
ν	A fixed constant representing how tightly singing whales pack
f	Fraction of singing time, or "duty cycle," for a whale
f	Natural acoustic frequency (Hz)
J_0	Zeroth-order Bessel function of the first kind
k	Medium wavenumber at frequency f
k_r	Real part of the modal horizontal wavenumber
$k_{r,m}$	Horizontal wavenumber for mode m
I	Ambient noise power spectral density in terms of linear units (μPa^2/Hz)
I_{dB}	Ambient noise intensity in decibel (logarithmic) units
N	Number of singing whales present in region A
ω	Radial frequency
P (and p)	A variable denoting a collection of acoustic propagation factors
ψ_m	Depth amplitude function for mode m
Q_{indiv}	Changes in an individual whale's singing behavior in response to a fractional change in the population size around it
Q_m	Normalized source spectrum
q	Source strength in source intensity spectral density per unit area
R	Radius of region A
r	Horizontal range of a given noise source to the hydrophone
ρ	Water density
S	Source spectral density in μPa^2/Hz @ 1 m
S_{dB}	Source spectral density in decibel (logarithmic) units
σ	Spatial density of singing whales
γ	Coefficient of the categorical variable for year in the GLM
Z_w	Depth of singing whales
Z_r	Depth of the recorder

APPENDIX A: THE KUPERMAN-INGENITO-PERKINS (KIP) MODEL

A propagating acoustic field in an ocean with a relatively flat bathymetry can be modeled as the weighted sum of a set of normal modes,

$$p(f, z_w, z_r, S) = \frac{S(f)}{\rho}\sqrt{\frac{2\pi}{r}}\sum_m \frac{e^{ik_{r,m}r}}{\sqrt{k_{r,m}}}\psi_{m(z_w)}\psi_{m(z_r)}, \tag{A1}$$

where S is the *linear* source intensity (in W/m^2, *not* dB re 1 μPa) of a sound produced at water depth z_w and horizontal range r. Additionally, ρ is the water density, k is the medium wavenumber at frequency f, ψ_m, and $k_{r,m}$ are the mode depth function ("mode") and horizontal wavenumber for index m, and z_r is the receiver depth. Roughly speaking, a mode represents a particular "multipath" that can travel a sustained horizontal distance in the ocean. The normal mode formulation is the most compact way to express the acoustic field for relatively low-frequency sounds in a shallow-water environment, with one caveat: in an actual ocean environment a continuous wavenumber contribution to the field exists at close ranges, and is an important contributor to the ambient noise field. This near-field contribution can be modeled using normal modes by adding a "false bottom" some distance beneath the actual ocean/sediment interface (Perkins *et al.*, 1993). This process yields a set of highly attenuated "leaky" modes that approximates this near-field contribution. Therefore, to remove the need to simulate a "false bottom," the simulations discussed in Sec. II D model an environment with a sediment layer overlying granite bedrock.

Kuperman and Ingenito (1980) showed that the cumulative noise field generated by a collection of temporally and spatially uncorrelated noise sources, each modeled with Eq. (A1), and all randomly distributed with respect to range and azimuth relative to the receiver, produces an analytical solution for sources distributed out to an infinite range. Perkins *et al.* (1993) extended this result for noise sources distributed over a finite range, producing the following equation for the ocean waveguide ambient noise power spectral density detected at the origin by a set of random sources distributed within a circular region of radius R surrounding the origin,

$$I(f,z_w,z_r,R)=q^2\left\{\frac{i\pi}{\rho^2k^2}\sum_{n,m}\frac{\psi_{n(z_w)}\psi_{m(z_w)}\psi_{n(z_r)}\psi_{m(z_r)}}{k_{r,m}^2-\left(k_{r,n}^*\right)^2}\times\left[2-\left(\sqrt{\frac{k_{r,m}}{k_{r,n}^*}}+\sqrt{\frac{k_{r,n}^*}{k_{r,m}}}\right)e^{-i\left(k_{r,m}-k_{r,n}^*\right)R}\right]\right\}. \tag{A2}$$

Here q^2represents a source strength in terms of units of source intensity spectral density per unit area. The term in curly brackets is the propagation term P in Eq. (1), and consists of a double sum of various weightings of normal modes. Note that this "regional radius" R does *not* represent the range between an individual singing whale and the receiver; rather, it represents the farthest range that any singing whale could be present at the time of the measurement.

As noted in previous literature, the double sum in Eq. (A2) can be approximated by a single sum by noting that the off-diagonal terms ($n \neq m$) are typically much smaller than the diagonal terms ($n=m$). The P term in Eq. (1) then becomes

$$P(f,z_w,z_r,R)\approx\frac{1}{\rho^2k^2}\sum_m\frac{\left(\psi_{m(z_w)}\psi_{m(z_r)}\right)^2}{2\kappa_m\alpha_m}\times\left[1-\frac{\kappa_m}{\sqrt{\alpha_m{}^2+\kappa_m{}^2}}e^{-2\alpha_mR}\right] \tag{A3}$$

or defining $U_m\equiv\left[\psi_m(z_w)\psi_m(z_r)\right]^2$ and $T_m\equiv\kappa_m/\sqrt{\alpha_m{}^2+\kappa_m{}^2}$,

$$P(f,z_w,z_r,R)\approx\sum_m\frac{U_m(z_w,z_r)}{2\kappa_m\alpha_m}\left[1-T_me^{-2\alpha_mR}\right]. \tag{A4}$$

Here κ_m and α_m are the real and imaginary parts of the horizontal wavenumber $k_{r,m}$ of mode m: $k_{r,m}=\kappa_m+i\alpha_m$. The imaginary term expresses the attenuation factor (how rapidly the mode decays with horizontal propagation distance) for the mode in question. Equation (A4) shows that the P term in Eq. (1) asymptotically approaches a fixed value as R becomes infinite, as long as some non-zero attenuation α_m exists in the propagation medium. Figure 11 reproduces Fig. 3(a), but uses all terms in the double sum [Eq. (A2)] instead of just the "diagonal" terms [Eq. (A3)]. A comparison of the figures shows that the dB contours of the simplified expression are virtually identical to the complete expression of Eq. (A2), although the contours display more fine-scaled structure with R. When δ_{CD} is estimated in the (bandwidth-integrated) manner shown in Fig. 4, the resulting sensitivity estimates are unchanged.

To compute the term dP/dR in Eq. (5b) we take the partial derivative of Eq. (A3) with respect to R and find

$$\frac{\partial P}{\partial R}=\sum_m\frac{U_m}{\kappa_m}T_me^{-2\alpha_mR}. \tag{A5}$$

Thus the second term in Eq. (5b) [or third term in Eq. (4)] becomes

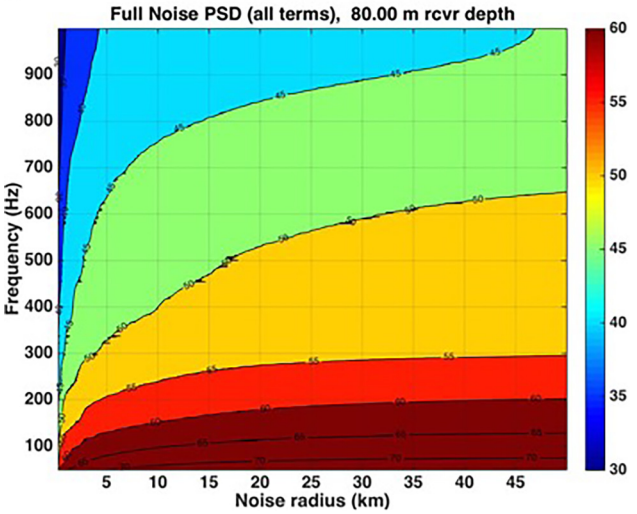

FIG. 11. (Color online) Reproduction of Fig. 3(a), but using all double summation terms in Eq. (A2) instead of the single-summation approximate form of Eqs. (A3) and (A4). The colorbar units are in terms of power spectral density: dB re 1 μPa^2/Hz.

$$\left(\frac{\nu R}{2P}\right)\frac{\partial P}{\partial R}=\frac{\nu R\sum_m\frac{U_m}{\kappa_m}T_me^{-2\alpha_mR}}{\sum_m\frac{U_m}{\kappa_m\alpha_m}\left[1-T_me^{-2\alpha_mR}\right]} \tag{A6}$$

and approaches a maximum value of $\nu/2$ (1/2 when $\nu=1$) for situations where both R and α_m are small, such that $T_m \sim 1$, $e^{-2\alpha R}\sim 1$, and $1-T_me^{-2\alpha R}\sim 2\alpha R$. Similar expressions can be obtained for the full double-sum expression for P in Eq. (A2).

Equations (A1)–(A6) have assumed that the receiver is placed at the center of the noise area A. When the receiver location is placed at an offset ΔR meters with respect to the geographic center of the noise-producing region, Eq. (A2) is modified to become

$$I(f,z_w,z_r,R)=q^2\left\{\frac{i\pi}{\rho^2k^2}\sum_{n,m}\frac{\psi_{n(z_w)}\psi_{m(z_w)}\psi_{n(z_r)}\psi_{m(z_r)}}{k_{r,m}^2-\left(k_{r,n}^*\right)^2}\times\left[2-J_0\left[\left(k_{r,m}-k_{r,n}^*\right)\Delta R\right]\times\left(\sqrt{\frac{k_{r,m}}{k_{r,n}^*}}+\sqrt{\frac{k_{r,n}^*}{k_{r,m}}}\right)e^{-i\left(k_{r,m}-k_{r,n}^*\right)R}\right]\right\}. \tag{A7}$$

One sees that, in cross-modal terms (where $n\neq m$), the term associated with T_m is modified by a zeroth-order Bessel function J_0. However, the approximate single-sum expressions in Eqs. (A4)–(A6) remain unmodified, since $J_0(0)=1$. Thus if an acoustic receiver lies anywhere within the boundary of the singing region, Fig. 3(a) will look roughly the same. Only the fine scale structure of the contour lines will shift. These results also imply that narrowband empirical measurements of sensitivity are robust to the receiver location within the singing area.

APPENDIX B: GENERALIZING THE MODEL FOR VARIATIONS IN SOURCE LEVEL, SINGING DEPTH, BROADBAND VOCALIZATIONS, AND SPATIAL DENSITY GRADIENTS

Equation (1) is defined for power spectral density (or intensity integrated across a narrow frequency band) and assumes a group of randomly distributed animals that share the same source levels and singing depths. Here we show that the key consequences of the model are retained when these assumptions are relaxed.

A better model of humpback whale singing behavior consists of defining a probability density function $p(S,z_w)$ such that out of a total population $N_{singers}$, the number of animals singing between depth $z_w \pm \Delta z/2$ with (linear) source intensity spectral densities between $S \pm \Delta S/2$ will be $\sim N_{singers} p(S,z_w)\Delta z \Delta S$. If we can factor $p(S,z_w)$ into $p(S)p(z_w)$ (i.e., assume that source level is statistically independent of singing depth), then a little thought shows that Eq. (1) remains valid if S is replaced by

$$\bar{S} = \int_0^\infty S p(S) dS \tag{B1}$$

and Eq. (A4) remains valid if is replaced by

$$\overline{U_m} \equiv [\psi_m(z_r)]^2 \int_0^\infty p(z_w)\psi_m^2(z_w)dz. \tag{B2}$$

Note that Eq. (B1) is defined over the *linear* source level, so if a source level distribution is presented in terms of dB, $\bar{S}$ will likely be dominated by the upper tail of the distribution.

With these modifications one can proceed through Eqs. (2)–(5) and find that δ in Eq. (7) is still independent of $\bar{S}$. If $p(S,z_w)$ cannot be factored, because source levels change with calling depth, then δ will depend on the functional relationship between S and $z_{w,}$ unless most animals are calling at similar depths. There are at least two reasons why factoring source level from calling depth might not be a reasonable assumption: (1) increasing static pressure with depth may make sound production more difficult, thus decreasing source level with depth; (2) if resonances are involved in sound production, these resonances may also be pressure-dependent.

Another correction to Eq. (1) is the incorporation of a broadband integration into the intensity measurement (instead of the narrowband integrations shown in Fig. 4). If the time-averaged spectrum from a singing whale, including periods of silence between units, is independent of its broadband source level, i.e., $S(\omega)$ is independent of $\sqrt{\int_{\omega_1}^{\omega_2} d\omega |S(\omega)|^2}$, then the definition of the sensitivity in Eq. (3) can be expanded to involve an incoherent summation across a bandwidth defined by frequencies ω_1 and ω_2. Thus, using Eqs. (3) and (A6), an example of the sensitivity for the constant density scenario becomes

$$\delta_{broadband} \equiv \frac{\partial(I_{dB,broadband})}{\partial(10\log_{10}N)} = Q_{indiv} + \frac{\nu R \int_{\omega_1}^{\omega_2} \frac{\overline{Q(\omega)}}{k^2}\left[\sum_m \frac{\overline{U_m}}{\kappa_m} T_m e^{-2\alpha_m R}\right] d\omega}{\int_{\omega_1}^{\omega_2} \frac{\overline{Q(\omega)}}{k^2}\left[\sum_m \frac{\overline{U_m}}{\kappa_m \alpha_m}\left[1 - T_m e^{-2\alpha_m R}\right]\right] d\omega}. \tag{B3}$$

Here $\overline{Q_\omega} = S(\omega)/\sqrt{\int_{\omega_1}^{\omega_2} d\omega |S(\omega)|^2}$. As before, the sensitivity δ from a broadband noise intensity measurement will be independent of the distribution-averaged individuals source levels $S_{dB,broadband}$. The difference from before, though, is that the modal terms are now weighted by $\overline{Q_\omega}$ (the normalized source spectrum).

Finally, the propagation term P in Eq. (1) is independent of azimuth in a range-independent environment. An immediate consequence of this fact is that Eq. (1) is a solution not only for constant spatial densities of animals, but is also a solution for scenarios where animals are distributed along a linear spatial gradient. Let $\sigma(r,\theta) = N/A(N)$ be the spatial density of singing animals at range r and azimuth θ from the sensor. Then Eq. (1) shows that the contribution to the ambient noise field from an annular ring of sources between r and $r + dr$ is proportional to $\int_0^{2\pi} \sigma(r,\theta) r dr d\theta$. For an arbitrary linear spatial gradient $\sigma = \sigma_0 + mr\cos\theta$ (where σ_0 is the spatial density directly over the sensor and m is the linear spatial gradient), one finds

$$\int_0^{2\pi} \sigma(r,\theta) r dr d\theta = \int_0^{2\pi} \sigma_0 r dr d\theta. \tag{B4}$$

Since Eq. (B4) holds for any annular ring of radius r, Eq. (1) is a solution for a distribution of noise sources with a linear spatial gradient, provided the spatial density used in Eq. (1) is the spatial density of noise sources directly above the sensor.

In summary, the expanded definition of δ in Eq. (B3) remains independent of the population's source level distribution and duty cycle under the following two assumptions: (1) the source levels generated by a population are statistically independent of their singing depths, and (2) the spectral shape of the animals' song spectrum (averaged across the entire duration of the song, including silent periods) is independent of the broadband source level. Extensions of the theory to cover a distribution of duty cycles (periods of rest) are straightforward. The sensitivity is also unaffected by the presence of a linear spatial gradient in the spatial distribution of singers. Three major assumptions remain that cannot be relaxed without resorting to full numerical simulations: (1) the songs must be temporally uncorrelated over the measurement window, (2) the singing area is a circular wedge, and (3) the bathymetry under the singing region is flat.

Au, W. W. L., Mobley, J., Burgess, W. C., and Lammers, M. O. (**2000**). "Seasonal and diurnal trends of chorusing humpback whales wintering in waters off Western Maui," Marine Mammal Sci. **16**(3), 530–544.

Baker, C. S., and Herman, L. M. (**1984**). "Aggressive behavior between humpback whales (*Megaptera novaeangliae*) wintering in Hawaiian waters," Can. J. Zoology **62**, 1922–1937.
Barlow, J., and Taylor, B. L. (**2005**). "Estimates of sperm whale abundance in the northeastern temperate Pacific from a combined acoustic and visual survey," Marine Mammal Sci. **21**(3), 429–445.
Blumstein, D. T., Mennill, D. J., Clemins, P., Girod, L., Yao, K., Patricelli, G., Deppe, J. L., Krakauer, A. H., Clark, C., Cortopassi, K. A., Hanser, S. F., McCowan, B., Ali, A. M., and Kirschel, A. N. G. (**2011**). "Acoustic monitoring in terrestrial environments using microphone arrays: Applications, technological considerations and prospectus," J. Appl. Ecol. **48**, 758–767.
Buckland, S. T. (**2006**). "Point transect surveys for songbirds: Robust methodologies," Auk **123**, 345–357.
Calambokidis, J., Falcone, E. A., Quinn, T. J., Burdin, A. M., Clapham, P. J., Ford, J. K. B., Gabriele, C. M., LeDuc, R., Mattila, D., Rojas-Bracho, L., Straley, J. M., Taylor, B. L., Urbán-R. J., Weller, D., Witteveen, B. D., Yamaguchi, M., Bendlin, A., Camacho, D., Flynn, K., Havron, A., Huggins, J., Maloney, N., Barlow, J., and Wade, P. R. (**2008**). "SPLASH: Structure of populations, levels of abundance and status of humpback whales in the north pacific," final report for Contract No. AB133F-03-RP-00078 prepared by Cascadia Research for U.S. Department of Commerce.
Charif, R. A., Clapham, P. J., and Clark, C. W. (**2001**). "Acoustic detections of singing humpback whales in deep waters off the British Isles," Marine Mammal Sci. **17**, 751–768.
Cholewiak, D. M. (**2008**). "Evaluating the role of song in the humpback whale (*Megaptera novaengliae*) breeding system with respect to intrasexual interactions," Doctoral thesis, Cornell University, Ithaca, NY.
Clapham, P. J., and Mattila, D. K. (**1990**). "Humpback whale songs as indicators of migration routes," Marine Mammal Sci. **6**, 155–160.
Clark, C. W., and Clapham, P. J. (**2004**). "Acoustic monitoring on a humpback whale (*Megaptera novaeangliae*) feeding ground shows continual singing into late spring," Proc. R. Soc. London, Ser. B **271**, 1051–1057.
Clark, C. W., and Fristrup, K. M. (**1997**). "Whales'95: A combined visual and acoustic survey of blue and fin whales off southern California," Rep. Int. Whaling Commission **47**, 583–600.
Darling, J. D., and Bérubé, M. (**2001**). "Interactions of singing humpback whales with other males," Marine Mammal Sci. **17**, 570–584.
Dawson, D. K., and Efford, M. G. (**2009**). "Bird population density estimated from acoustic signals," J. Appl. Ecol. **46**, 1201–1209.
Dedina S. (**2014**). (personal communication).
Dunlop, R. A., Cato, D. H., and Noad, M. J. (**2008**). "Non-song acoustic communication in migrating humpback whales (*Megaptera novaeangliae*)," Marine Mammal Sci. **24**(3), 613–629.
Frankel, A. S., Clark, C. W., Herman, L. M., and Gabriele, C. M. (**1995**). "Spatial distribution, habitat utilization, and social interactions of humpback whales, *Megaptera novaeangliae*, off Hawai'i, determined using acoustic and visual techniques," Can. J. Zoology **73**, 1134–1146.
Gavrilov, A. N., and McCauley, R. D. (**2013**). "Acoustic detection and long-term monitoring of pygmy blue whales over the continental slope in southwest Australia," J. Acoust. Soc. Am. **134**(3), 2505–2513.
Hamilton, E. L. (**1980**). "Geoacoustic modeling of the sea floor," J. Acoust. Soc. Am. **68**, 1313–1339.
Jensen, F. B., Kuperman, W. A., Porter, M. B., and Schmidt, H. (**1994**). *Computational Ocean Acoustics* (AIP, New York).
Jiménez-López, M. E. (**2006**). "Uso de hábitat de madres con cría y machos cantores de ballena jorobada (*Megaptera novaeangliae*), en la region Los Cabos, Baja California Sur, durante el invierno 2004" ("Habitat use by humpback whale mothers and calves with singing males, in the Los Cabos, Baja California Sur region, during the 2004 winter"), M.S. thesis, Universidad Autónoma de Baja California Sur, La Paz, Baja California Sur, Mexico.
Kuperman, W. A., and Ingenito, F. (**1980**). "Spatial correlation of surface generated noise in a stratified ocean," J. Acoust. Soc. Am. **67**, 1988–1996.
Luczkovich, J. J., Mann, D. A., and Rountree, R. A. (**2008**). "Passive acoustics as a tool in fisheries: An introduction to the American Fisheries Society Symposium," Trans. Am. Fisheries Soc. **137**, 533–541.
Marques, T. A., Munger, L., Thomas, L., Wiggins, S., and Hildebrand, J. A. (**2011**). "Estimating North Pacific right whale *Eubalaena japonica* density using passive acoustic cue counting," Endangered Species Res. **13**, 163–172.
Marques, T. A., Thomas, L., Martin, S. W., Mellinger, D. K., Ward, J. A., Moretti, D. J., Harris, D., and Tyack, P. L. (**2013**). "Estimating animal population density using passive acoustics," Biol. Rev. **88**, 287–309.
Marques, T. A., Thomas, L., Ward, J., DiMarzio, N., and Tyack, P. L. (**2009**). "Estimating cetacean population density using fixed passive acoustic sensors: An example with Blainville's beaked whales," J. Acoust. Soc. Am. **125**, 1982–1994.
Martin, S. W. (**2013**). "Estimating minke whale (*Balaenoptera acutorostrata*) boing sound density using passice acoustic sensors," Marine Mammal Sci. **29**(1), 142–158.
Mattila, D. K., Guinee, L. N., and Mayo, C. A. (**1987**). "Humpback whale songs on a North Atlantic feeding ground," J. Mammal. **68**, 880–883.
McCauley, R. D., Jenner, C., Bannister, J. L., Burton, C. L. K., Cato, D. H., and Duncan, A. (**2001**). "Blue whale calling in the Rottnest Trench—2000," Western Australia, Curtin University Perth Project Cmst., p. 241.
McDonald, M. A., and Fox, C. G. (**1999**). "Passive acoustic methods applied to fin whale populations density estimation," J. Acoust. Soc. Am. **105**(5), 2643–2651.
Mednis, A. (**1991**). "An acoustic analysis of the 1988 song of the humpback whale, *Megaptera novaeangliae*, off Eastern Australia," Mem. Queensland Museum **30**, 323–332.
Mellinger, D. K., and Barlow, J. (**2003**). "Future directions for marine mammal acoustic surveys: Stock assessment and habitat use," report of a workshop held in La Jolla, CA, November 20–22, 2002, technical contribution No. 2557, NOAA Pacific Marine Environmental Laboratory, Seattle, WA.
Mellinger, D. K., Küsel, E. T., Thomas, L., and Marques, T. A. (**2009**). "Taming the Jez monster: Estimating fin whale spatial density using acoustic propagation modeling," J. Acoust. Soc. Am. **126**, 2229.
Nishiwaki, M. (**1959**). "Humpback whales in Ryukyuan waters," Sci. Rep. Whales Res. Inst., Tokyo **14**, 49–87.
Norris, T. F., Jacobsen, J. K., and Cerchio, S. (**2000**). "A comparative analysis of humpback whale songs recorded in pelagic waters of the Eastern North Pacific: Preliminary findings and implications for discerning migratory routes and assessing breeding stock identity," NOAA technical memorandum, U.S. Department of Commerce, San Diego, CA.
Norris, T. F., McDonald, M., and Barlow, J. (**1999**). "Acoustic detections of singing humpback whales (*Megaptera novaeangliae*) in the eastern North Pacific during their northbound migration," J. Acoust. Soc. Am. **106**, 506–514.
Payne, K., and Payne, R. (**1985**). "Large scale changes over 19 years in songs of humpback whales in Bermuda," Z. Tierpsychol. **68**, 89–114.
Payne, R., and McVay, S. (**1971**). "Songs of humpback whales," Science **173**, 585–597.
Perkins, J. S., Kuperman, W. A., Ingenito, F., Fialkowski, L. T., and Glattetre, J. (**1993**). "Modeling ambient noise in three-dimensional ocean environments," J. Acoust. Soc. Am. **92**, 739–752.
Ponce, D., Thode, A. M., Guerra, M., Urban, J., and Swartz, S. (**2012**). "Relationship between visual counts and call detection rates of gray whales (*Eschrichtius robustus*) in Laguna San Ignacio, Mexico," J. Acoust. Soc. Am. **131**(4), 2700–2713.
Raftery, A. E., and Zeh, J. E. (**1998**). "Estimating bowhead whale population size and rate of increase from the 1993 census," J. Am. Stat. Assoc. **93**(442), 451–463.
Sharpe, F. (**2001**). "Social foraging of the Southeast Alaskan humpback whale, *Megaptera novaeangliae*," Ph.D. thesis, Simon Fraser University, Burnaby, British Columbia, Canada.
Sousa-lima, R. S., and Clark, C. W. (**2008**). "Modeling the effect of boat traffic on the fluctuation of humpback whale singing activity in the Abrolhos National Marine Park, Brazil," Can. Acoust. **36**, 175–181.
Stimpert, A. K., Au, W. W. L., Parks, S. E., Hurst, T., and Wiley, D. N. (**2011**). "Common humpback whale (*Megaptera novaeangliae*) sound types for passive acoustic monitoring," J. Acoust. Soc. Am. **129**(1), 476–482.
Stimpert, A. K., Peavey, L. E., Friedlaender, A. S., and Nowacek, D. P. (**2012**). "Humpback whale song and foraging behavior on an Antarctic feeding ground," PLoS One **7**, e51214.
Tyack, P. (**1981**). "Interactions between singing Hawaiian humpback whales and conspecifics nearby," Behav. Ecol. Sociobiol. **8**, 105–116.
Vu, E. T., Risch, D., Clark, C. W., Gaylord, S., Hatch, L. T., Thompson, M. A., Wiley, D. N., and Van Parijs, S. M. (**2012**). "Humpback whale song occurs extensively on feeding grounds in the western North Atlantic Ocean," Aquat. Biol. **14**, 175–183.
Winn, H. E., and Winn, L. K. (**1978**). "The song of the humpback whale, *Megaptera novaeangliae*, in the West Indies," Marine Biol. **47**, 97–114.
Zoidis, A. M., Smultea, M. A., Frankel, A. S., Hopkins, J. L., Day, A., McFarland, A. S., Whitt, A. D., and Fertl, D. (**2008**). "Vocalizations produced by humpback whale (*Megaptera novaeangliae*) calves recorded in Hawaii," J. Acoust. Soc. Am. **123**(3), 1737–1746.